Aeroacoustic source characterization at fan test facility with spherical harmonics of the half-space

JASA EXPRESS LETTERS ARTICLE asa.scitation.org/journal/jel

Aeroacoustic source characterization at fan test facility with spherical harmonics of the half-space

Michail Vourakis,[1] Franz Zotter,[2] Eric Brandão,[3] and Elias Zea[4,a)]
[1]Department of Mechanics and Maritime Sciences, Division of Fluid Dynamics, Chalmers University of Technology, Hörsalsvägen 7A, 412 96 Gothenburg, Sweden
[2]Institute of Electronic Music and Acoustics, University of Music and Performing Arts, Inffeldgasse 10/3, 8010 Graz, Austria
[3]Acoustical Engineering, Federal University of Santa Maria, Santa Maria-RS, 97050-140, Brazil
[4]KTH Royal Institute of Technology, Department of Engineering Mechanics, The Marcus Wallenberg Laboratory for Sound and Vibration Research, Teknikringen 8, 100 44 Stockholm, Sweden
michail.vourakis@chalmers.se, zotter@iem.at, eric.brandao@eac.ufsm.br, zea@kth.se

Abstract: Acoustic measurements of sources in non-ideal acoustic environments, often the case in industrial product development, issue challenges in source characterization. This study investigates the room-acoustical effects of a bespoke fan test facility on aeroacoustic source characterization via a second-order scheme of spherical harmonics of the half-space. An experimental test of a compact monopole-like sound source reveals the influence of the room's transfer function at low frequencies. Applying the scheme to a benchmark case of a low-pressure axial fan at different loading conditions showcases a satisfactory estimation of sound power and directivity.

[Editor: Con Doolan] https://doi.org/10.1121/10.0036723

Received: 18 March 2025 **Accepted:** 29 April 2025 **Published Online:** 16 May 2025

1. Introduction

Aeroacoustic measurements necessitate low background noise and minimal influence of the room's reflections for high accuracy. The current landscape of wind tunnel facilities capable of such measurements can be broadly divided based on their test section. Open-jet sections allow the acoustic treatment of surrounding boundaries, placement of microphones outside the main flow, and low levels of background noise; thus, they have been utilized for a multitude of experimental studies, including airfoils (Botero-Bolívar *et al.*, 2024; Bowen *et al.*, 2022), rotors (Torija *et al.*, 2022; Chen *et al.*, 2020), and propellers (Torija *et al.*, 2021; Turhan *et al.*, 2024). Close-test sections favor better flow control and validation with numerical models (Merino-Martínez *et al.*, 2019; Niu *et al.*, 2022), while the absence of a shear layer enables accurate acoustic source localization. However, microphones can be exposed to flow-induced self-noise and source-unrelated sound waves, which can propagate to the test section due to hard walls. Consequently, the source characterization process deteriorates with the influence of coherent reflections and uncorrelated background noise. These issues can be minimized by modifying the test section (Defreitas and Alexander, 2023) and/or by using array processing techniques (Koop and Ehrenfried, 2008).

The sound field of a variety of aeroacoustic sources can be described via spherical harmonic decomposition (SHD). Recently, subsonic jet noise was characterized via spherical harmonics (Dreier *et al.*, 2023). The approach showcased a higher signal-to-noise ratio for the corresponding numerical resolution limit compared to previous studies and indicated the microphone number requirement towards a fully resolved sound field. The sound fields of canonical rotating aeroacoustic sources, namely, monopoles (Poletti and Teal, 2011), dipoles (Mao *et al.*, 2012), and quadrupoles (Mao *et al.*, 2014) have also been extensively studied and validated numerically. Furthermore, SHD has been utilized in beamforming methods concerning directional sources (Bouchard *et al.*, 2011) and rotating sound sources in the frequency domain (Ocker and Pannert, 2017) or in the time domain (Ma *et al.*, 2023). A case study on drone noise (Alkmim *et al.*, 2022) was based on an SHD of hemispherical microphone array data measured at a hemi-anechoic chamber. The SHD of the drone's acoustic near-field allowed the study of the directivity and psychoacoustics of the acoustic far field. Despite the lack of a complete aeroacoustic characterization, the effect of the floor's reflections was minimized by installing foam material.

This study aims to achieve two goals. First, it aims to identify room-acoustical effects, including the floor's reflections, for a fan test facility (FTF) based on a second-order SHD of the far-field sound pressure radiated by a reference

a)Author to whom correspondence should be addressed.

monopole source. It should be noted here that the implemented SHD concerns a half-space. Second, it aims to evaluate the use of the SHD to characterize the sound field of a low-speed axial fan in terms of its directivity and sound power.

2. Methodology

2.1 Acoustic monopole on a rigid half-space

Let us consider a point monopole source radiating in a free field over a reflecting surface. Using the image source principle (Allen and Berkley, 1979) the total sound pressure field in Pa at a given observation point $\mathbf{r} = (x, y, z)$ and angular frequency ω is

$$p(\mathbf{r}, \omega) = \frac{\rho \mathrm{j}\omega Q_0}{4\pi}\left(\frac{\mathrm{e}^{-\mathrm{j}k|\mathbf{r}-\mathbf{r}_0|}}{|\mathbf{r}-\mathbf{r}_0|} + \frac{\mathrm{e}^{-\mathrm{j}k|\mathbf{r}-\mathbf{r}_0'|}}{|\mathbf{r}-\mathbf{r}_0'|}\right), \tag{1}$$

where $k = \omega/c$ in rad/m is the acoustic wavenumber, ρ is the air density in kg/m^3, j is the imaginary unit, c is the speed of sound in m/s for ambient conditions, $\mathbf{r}_0 = (x_0, y_0, z_0)$ are the point source coordinates, $\mathbf{r}_0' = (x_0, y_0, -z_0)$ are the image source coordinates, and Q_0 is the point source's strength in m^3/s. The assumed time dependence is $\mathrm{e}^{\mathrm{j}\omega t}$, omitted throughout.

2.2 SHD

The sound pressure field in Eq. (1) is expanded in spherical harmonics basis functions. Only half-space is considered due to the boundary conditions imposed at the acoustic environments tested in this Letter. Then, according to Zotter *et al.* (2007), it is possible to use only the even spherical harmonics Y_n^{2l-n} as basis functions for decomposition, which include the zeroth order term, corresponding to an acoustic monopole in a free field.

The complex-valued spherical harmonics $Y_n^m(\theta, \phi)$ of order n and degree m are defined as (Williams, 1999)

$$Y_n^m(\theta, \phi) = \sqrt{\frac{(2n+1)(n-|m|)!}{4\pi(n+|m|)!}} P_n^{|m|}(\cos\theta)\mathrm{e}^{\mathrm{j}m\phi}, \tag{2}$$

where P_n^m are the associated Legendre functions, θ is the zenith angle, and ϕ is the azimuth angle. Then, the SHD of the sound pressure at a certain radius r is written as (Williams, 1999)

$$p(kr, \theta, \phi) = \sum_{n=0}^{\infty}\sum_{m=-n}^{n} Y_n^m(\theta, \phi)\,\psi_{mn}(kr), \tag{3}$$

where ψ_{mn} is the n-th order spherical harmonic coefficient of degree m, and for the even harmonics, with $m = 2l - n$, $l = 0, \ldots, n$, it is regarded to be non-zero.

In a measurement scenario, the sound pressure is measured at a discrete set of M locations $(\theta_\mathrm{i}, \phi_\mathrm{i})$ distributed over the surface of a hemisphere, and the infinite summation in Eq. (3) is truncated at order N, leading to a set of linear equations given by

$$\mathbf{p} = \mathbf{Y}\boldsymbol{\psi}, \tag{4}$$

where $\mathbf{p} \in \mathbb{C}^M$ is a vector of acoustic pressure at measurement points (M), $\mathbf{Y}$ is the $M \times [(N+1)(N+2)/2]$ matrix of even spherical harmonics at the corresponding measurement positions (M), and $\boldsymbol{\psi} \in \mathbb{C}[(N+1)(N+2)/2]$ is the vector of the corresponding spherical harmonic coefficients. The matrix $\mathbf{Y}$ is evaluated utilizing the MATLAB Spherical Harmonic Transform Library (Politis, 2016). Then, the overdetermined system is solved for $\boldsymbol{\psi}$ using a least squares approach.

For the benchmark case defined in Eq. (1), the analytic expression for $\psi_{mn}(kr)$, containing both the monopole (Zotter, 2009) and its image, is also considered:

$$\psi_{mn}(kr) = -\mathrm{j}k\,h_n^{(2)}(kr)\left[j_n(kr_0)\,Y_n^m(\theta_0, \phi_0) + j_n(kr_0')\,Y_n^m(\theta_0', \phi_0')\right], \tag{5}$$

where $h_n^{(2)}$ is the spherical Hankel function of the second kind, while (r_0, θ_0, ϕ_0) and $(r_0', \theta_0', \phi_0')$ are the spherical coordinates of the source and image source, respectively. An order limit of 40 was deemed sufficient for convergence.

Subsequently, the isotropy of the sound field is assessed as an indicator of room-acoustical effects. The isotropy is estimated at each frequency (f) using the decomposed [Eq. (4)] and analytically derived [Eq. (5)] harmonic coefficients according to the approach in Nolan *et al.* (2020) omitting the time-harmonic dependence,

$$\iota(f) = \frac{|\psi_{00}(f)|}{\sum_{n=0}^{\infty}\sum_{m=-n}^{n}|\psi_{mn}(f)|}. \tag{6}$$

2.3 Sound power level (SWL) estimates

The SWL from measurements at the FTF is first estimated according to ISO 3744 (ISO, 2010). Since the facility does not fulfill hemi-anechoic conditions, an environment correction (K_2) has to be accounted for. According to ISO 3744 (ISO, 2010), K_2 can be estimated using an absolute comparison test with a reference sound source (A.2). However, the spectrum of the noise source and the reference sound source must be similar, posing a substantial limiting factor for complex aeroacoustic sources like axial fans (Neise and Michel, 1994). Alternatively, three methods based on room absorption (A.3) can also be used (ISO 3744; ISO, 2010): the reverberation method (A.3.2), the two-surface method (A.3.3), and a direct method via a reference sound source (A.3.4).

In this Letter, the reverberation method is used for estimating SWL despite the FTF's dimensions not conforming entirely to the recommended dimensions by ISO 3744 (ISO, 2010). The method estimates the equivalent sound absorption area via Sabine's reverberation time,

$$K_2 = 10\log_{10}\left(1 + 4\frac{S}{A}\right), \tag{7}$$

where A is the room's equivalent sound absorption area in m^2 calculated by the Sabine reverberation time equation and S is the measurement surface in m^2 of a hemisphere as defined by ISO 3744 (ISO, 2010). The FTF's reverberation time was measured according to ISO 3382-2 (ISO, 2008). Then, the estimation of SWL follows:

$$SWL_{\text{rev}} = \bar{L}_{\text{p}} + 10\log_{10}\left(\frac{S}{S_0}\right) - K_2, \tag{8}$$

where $\bar{L}_{\text{p}}$ in dB, corresponds to the spatial average of sound pressure over microphones at the measurement surface, and S_0 is a reference surface of $1\ m^2$. The reference sound pressure is $20\ \mu$Pa.

An alternative method to estimate the SWL based on SHD is also assessed. This is a composite SWL estimator (Pomberger *et al.*, 2016), which combines a far-field estimate as suggested by ISO 3745 (ISO, 2012) and a near-field estimate based on SHD. An adjusted expression from Pomberger *et al.* (2016) is given in Eq. (9),

$$SWL_{\text{comp}} = 10\log_{10}\left(\min\left(\frac{1}{2\rho c}\frac{2\pi r^2}{M}\sum_{i=1}^{M}|p_i|^2,\ \frac{1}{2\rho c}\sum_{m,n}\frac{|\psi_{mn}|^2}{k^2|h_n^{(2)}(kr)|^2}\right)\right), \tag{9}$$

where p_i is the sound pressure in Pa at a measurement point. It is noted here that the first term inside the min operator of Eq. (9) assumes hemi-anechoic conditions.

2.4 Experimental setup

The FTF investigated in this study is an aerodynamic, plenum-to-plenum, closed-loop type. The test object (monopole source and/or fan) is installed at the interface dividing the two plenums. Measurements are conducted at the plenum upstream of the test object (pressure chamber).

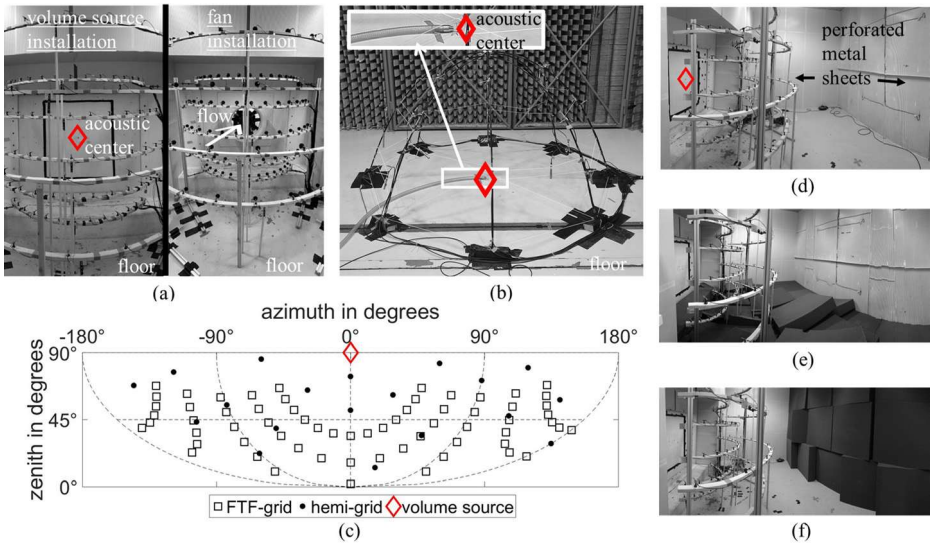

Fig. 1. Experimental setups of measurements at (a) FTF and (b) hemi-anechoic room. (c) Microphones and volume source positions in zenith-azimuth space. (d)–(f) Photographs of the FTF for different absorption material installations: (d) default, (e) floor, and (f) back wall absorption.

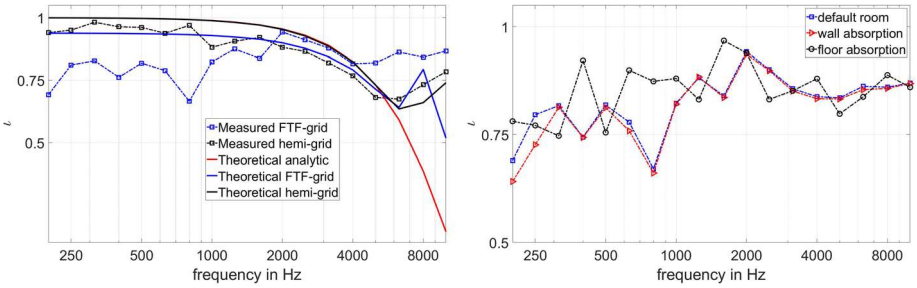

Fig. 2. (a) Isotropy of volume source (measured) and point monopole (theoretical), for hemi-anechoic and FTF microphone grid. (b) Isotropy of volume source for different absorption material installations at FTF.

The interface consists of a rectangular 1.2×1.3 m^2 plywood slab with 20 mm thickness over a concrete wall interface [see Figs. 1(a) and 1(d)]. The pressure chamber ($4.8 \times 3.1 \times 3$ m^3) features side walls with acoustic absorbent material behind a perforated metal sheet and an acoustically hard floor [see Fig. 1(d)]. Part of the measurements featured an extra layer of acoustic absorbent 200 mm thickness at the entry wall of the pressure chamber [see Fig. 1(e)] or the floor [see Fig. 1(f)]. According to the manufacturer, the utilized absorbent materials are described by a sound absorption coefficient of ∼0.8 at 200 Hz and ∼0.9 at 1000 Hz. Further information about the FTF can be found in Vourakis and Karlsson (2022). A hemi-anechoic room ($4.7 \times 7.5 \times 8.4$ m^3) with an acoustically hard floor is also utilized for part of the measurements [see Fig. 1(b)].

The sound source utilized in both acoustic environments (hemi-anechoic and FTF) is the Simcenter Qsources mid/high-frequency volume source. This source represents an acoustic monopole with omnidirectional characteristics. According to the manufacturer, the suggested frequency range for operating the source is 200–10 000 Hz. The sampling frequency is set at 51.2 kHz, while all signals are acquired via the data acquisition system Simcenter SCADAS Mobile. The excitation signal is white noise, and the acquisition time is set to 30 s. The recorded time signals are processed with the MATLAB built-in function `pwelch`, using 50% overlap, and a Hanning window size of 2^{16} samples. Further processing, according to Sec. 2, is performed for narrow-band and 1/3 octave band spectra.

Acoustic measurements of a low-pressure axial fan rotating at 1450 rpm are conducted at the FTF and compared to a publicly available dataset (Zenger *et al.*, 2016). More information about the measurement setup at the FTF is available from Vourakis and Karlsson (2022), while fan design parameters along with the measurement setup of the publicly available dataset can be found at Zenger *et al.* (2016).

Measurements at the hemi-anechoic room are recorded via 19 half-inch free-field microphones (Brüel & Kjaer type 4189; Brüel & Kjaer, Naerum, Denmark) positioned over the surface of a half sphere of 1 m radius. Positions are chosen according to ISO 3745 (ISO, 2012). Measurements at the FTF are recorded via 65 quarter-inch free-field microphones (G.R.A.S. type 40PH, GRAS, Holte, Denmark), installed over a spherical surface segment of the same radius. Figure 1 shows the different measurement setups in both acoustic environments and the microphone grids superimposed in zenith-azimuth space.

3. Results

3.1 Comparison between theoretical monopole and measured volume source

Figure 2(a) shows the isotropy metric $\iota(f)$ for the two acoustic environments as calculated for a theoretical point monopole source and the measured volume source over the corresponding microphone grids. Additionally, the isotropy curve corresponding to the analytic solution [see Eq. (5)] for an order limit of 40 is overlaid. Figure 2(b) depicts $\iota(f)$ for the volume source in the FTF over different absorption material installations. These results are estimated from the spectra in 1/3 octave bands to facilitate easier comprehension.

An aspect that affects the shape of the isotropy curve is the distance between the source and image source [see Eq. (1)]. Herein, the distance between the acoustic centers of the point source and the image source is set to 3 cm, following the manufacturer's information about the acoustic center of the utilized volume source. Increments in the distance result in the shift of the curve's first trough towards lower frequencies. This effect is more significant for the isotropy curves concerning the measurements since the utilized volume source is not a perfectly compact sound source, and the definition of its acoustic center is ambiguous. Nonetheless, the isotropy curve calculated from the measurements at the hemi-anechoic room demonstrates good qualitative agreement with the simulated point monopole, while amplitudes are comparable. On the contrary, the isotropy curve obtained from the measurements in the FTF reveals significant discrepancies compared to the simulated point monopole. The room-acoustical effects mainly impose these discrepancies, particularly at low frequencies. Moreover, the position uncertainty of the volume source's acoustic center is nontrivial due to the

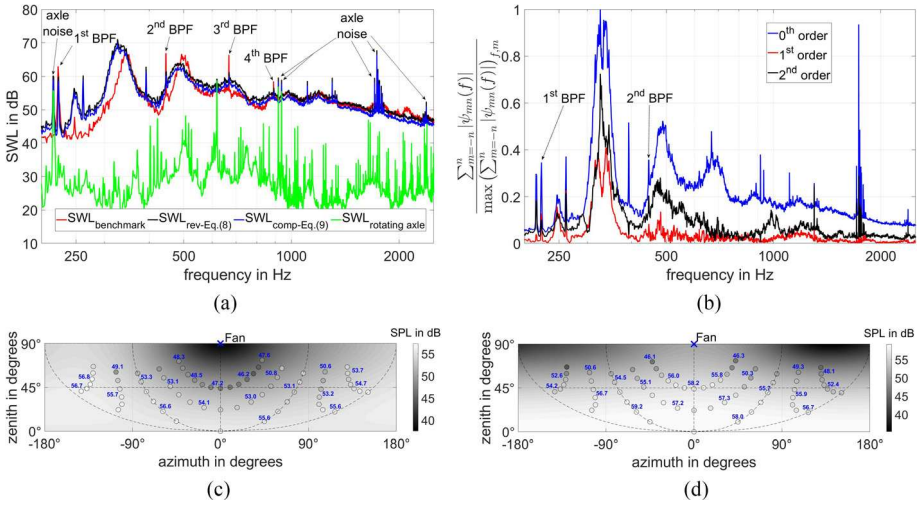

Fig. 3. (a) SWL of low-pressure axial fan with different estimators. (b) Sum of harmonic coefficients per order. (c) and (d) Sound pressure level directivity maps at (c) first and (d) second BPF and the design point.

presence of a plywood slab as the principal reflective surface, compared to the acoustically hard floor of the hemi-anechoic room.

The isotropy curve of the point monopole for the hemi-anechoic grid matches the curve of the analytic solution until ∼6.3 kHz. It can be assumed that existing interference patterns between the source and image source at high frequencies are not captured by a second-order limited scheme. Regardless, the occurrence of spatial aliasing (contamination by higher-order harmonics) is anticipated at these frequencies. The deviation between the point monopole cases of the FTF and hemi-anechoic grid can be attributed to the limited spatial range of the former. Additionally, the points of the FTF grid do not correspond to equal surface areas.

The effect of different absorption material installations in the FTF [see Figs. 1(e) and 1(f)] is demonstrated via the isotropy curves in Fig. 2(b). The effect of back wall installation is minimal since marginal discrepancies are observed compared to the default room case. On the contrary, the floor installation case features significant increments of isotropy at ∼400 Hz, across 550–1000 Hz and at ∼1800 Hz. These increments hint towards attenuating acoustic reflections at low frequencies, thereby minimizing room-acoustical effects. The isotropy levels of the same case across other frequencies are comparable to the default case.

It is remarked that deviations from the inverse square law for the FTF, not included here for brevity, violated allowable limits of a hemi-free field (ISO 3745; ISO, 2012), in certain 1/3 octave bands below 1 kHz. These deviations are considered to be in line with the observations made in agreement with the isotropy coefficient metric utilized in this study.

3.2 Application to a low-pressure axial fan

The estimated SWL of the low-pressure axial fan based on the considered estimators (see Sec. 2.3), at its design volumetric flow (VF) of 1.4 m^3/s and total-to-static pressure difference (PD) of 126.5 Pa, is presented in Fig. 3(a). Note that herein measurements correspond to the default FTF [see Fig. 1(d)], while the spectra are presented until 2.5 kHz due to increased noise contribution from the fan's driving axle (mainly bearings), as observed from the rotating axle's spectra ($SWL_{rotating\ axle}$) without the fan. The benchmark SWL from Zenger *et al.* (2016), measured in an anechoic chamber and estimated according to ISO 3744 (2010), is also included. The herein estimators exhibit marginal differences across the evaluated frequency range (200–10 000 Hz), which can be linked to the perceived measurement surface [see Eq. (9)]. Considering the near-field amplitudes included in the composite estimator, marginal improvement was observed compared to the benchmark data. Disregarding the instances of axle noise, discrepancies between FTF (both estimators) and benchmark data are mainly observed at low frequencies (230–330 Hz). This can be attributed to installation and geometry deviations of the fan and inlet shroud used in this study compared to the original shroud-fan system, along with different inlet flow conditions. Moreover, the inherent room-acoustical effects across low frequencies at the FTF, as observed in Sec. 3.1, may have a compounding effect.

The contribution of harmonic coefficients per order, concerning the near-field term based on SHD of the composite SWL estimator [see Eq. (9)], is shown in Fig. 3(b). Note that the sum of harmonic coefficients per order is non-dimensionalized with regard to the order-frequency combination of maximum amplitude. Overall, the evaluated orders exhibit qualitative similarity. The sum of the second-order term coefficients is comparable to that of the zeroth order until 500 Hz and around 1 kHz, while the sum of the first-order term coefficients is notably smaller. The significance of the

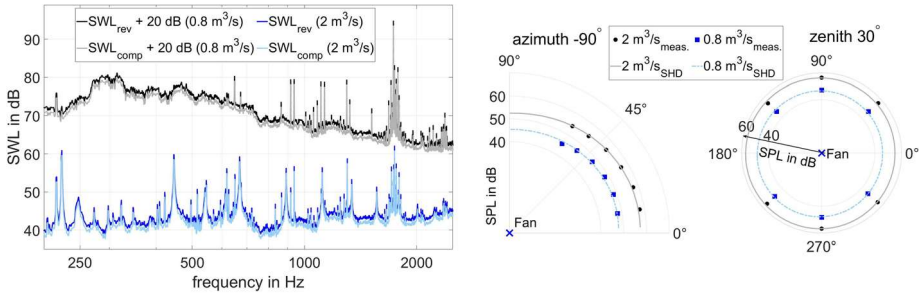

Fig. 4. (a) SWL of low-pressure axial fan based on different methods. (b) Reconstructed and measured SPL in polar coordinates for the first BPF at different loading conditions.

first-order terms at the first blade passing frequency (BPF) is higher than that of the second-order terms, which is consistent with the prevalence of rotating dipoles (i.e., first-order harmonic terms) at frequencies that are integer multiples of the fan's rotational speed. However, the contribution of the second-order terms at the second BPF is substantially higher than that of the first-order terms.

Figures 3(c) and 3(d) show the directivity maps at the first and second BPF obtained from reconstructing the sound pressure field over the half-space based on the estimated matrix of the spherical harmonics [see Eq. (4)]. The reconstruction is performed with a step of 5° over azimuth and zenith, while the sound pressure level (SPL) measured at the FTF grid is also overlaid. Overall, the reconstruction over the half-space retains the measured directivity pattern of the two BPFs despite the abrupt SPL changes measured across small angles.

The applicability of the SHD for the tested fan is further presented over different loading conditions. It should be noted that the benchmark study (Zenger *et al.*, 2016) does not contain time series data from other loading conditions. Thus, only results from the FTF are regarded here. Two operating points of higher (VF = 0.8 m^3/s and PD = 141 Pa) and lower (VF = 2 m^3/s and PD = 5 Pa) loading are considered. The former represents unsteady (stall) conditions, while the latter free discharge. The estimated SWL_{comp} of these operating points, according to Eq. (9), is shown in Fig. 4(a). The corresponding SWL_{rev} implementing Eq. (8) is also overlaid. Marginal differences are observed between the *SWL* spectra of the two methods across the frequency range presented for both operating scenarios. Finally, the reconstructed and measured SPL in polar coordinates for the first BPF at specific azimuth and zenith angles is presented in Fig. 4(b). The reconstructed SPL (gray and light blue curves) at the first BPF demonstrates good agreement compared to the discrete measurements (black dots and blue squares). Overall, these results highlight the effectiveness of the SHD for the half-space despite the imposed second-order limit and the presence of room-acoustical effects.

4. Summary

Aeroacoustic sources are characterized in a FTF via a SHD scheme of the half-space, second-order limited. Initially, the sound field of a monopole-like source is measured at a hemi-anechoic room and the FTF with different absorption material installations. The analysis of the source's isotropy levels indicates room-acoustical effects below ~1 kHz at the FTF. Furthermore, the SHD scheme is utilized for characterizing a low-pressure axial fan at the FTF. The sound power and the directivity of the fan, under different loading conditions, are estimated effectively over the frequency range 200–2500 Hz.

Acknowledgments

This work is part of the project eFan, a key enabler for eMobility, part II, and is funded by the Swedish Energy Agency, Grant No. 2020–016065. Volvo Group Trucks Technology is acknowledged for providing measurement facilities and equipment. The authors would like to acknowledge Karl Levenstam for designing and manufacturing the testing and measurement equipment and Erik Jenåker for conducting parts of the measurements.

Author Declarations

Conflict of Interest

The authors have no conflicts to disclose.

Data Availability

The data that support the findings of this study are available in Zenodo, https://zenodo.org/records/15292362 [https://doi.org10.5281/zenodo.15292361].

References

Alkmim, M., Cardenuto, J., Tengan, E., Dietzen, T., Van Waterschoot, T., Cuenca, J., De Ryck, L., and Desmet, W. (**2022**). "Drone noise directivity and psychoacoustic evaluation using a hemispherical microphone array," J. Acoust. Soc. Am. **152**(5), 2735–2745.

Allen, J., and Berkley, D. (**1979**). "Image method for efficiently simulating small-room acoustics," J. Acoust. Soc. Am. **65**, 943–950.

Botero-Bolívar, L., Dos Santos, F. L., Venner, C. H., and de Santana, L. D. (**2024**). "Trailing-edge far-field noise and noise source characterization in high inflow turbulence conditions," J. Acoust. Soc. Am. **155**(2), 803–816.

Bouchard, C., Havelock, D. I., and Bouchard, M. (**2011**). "Beamforming for directional sources: Additional estimator and evaluation of performance under different acoustic scenarios," J. Acoust. Soc. Am. **129**(4), 2042–2051.

Bowen, L., Celik, A., Zhou, B., Westin, M. F., and Azarpeyvand, M. (**2022**). "The effect of leading edge porosity on airfoil turbulence interaction noise," J. Acoust. Soc. Am. **152**(3), 1437–1448.

Chen, W., Peng, B., Liem, R. P., and Huang, X. (**2020**). "Experimental study of airfoil-rotor interaction noise by wavelet beamforming," J. Acoust. Soc. Am. **147**(5), 3248–3259.

Defreitas, A., and Alexander, W. N. (**2023**). "Identification of anomalies in microphone array measurements of trailing edge noise by eigenstructure analysis," J. Acoust. Soc. Am. **153**(2), 1073–1083.

Dreier, C., Vogt, X., Schröder, W., and Vorländer, M. (**2023**). "Acoustic source characterization of simulated subsonic jet noise using spherical harmonics," J. Acoust. Soc. Am. **154**(1), 167–178.

ISO (**2008**). ISO 3382, "Acoustics—Measurement of room acoustic parameters—Part 2: Reverberation time ordinary rooms" (ISO, Geneva, Switzerland).

ISO (**2010**). ISO 3744:2010, "Acoustics—Determination of sound power levels and sound energy levels of noise sources using sound pressure—Engineering methods for an essentially free field over a reflecting plane" (ISO, Geneva, Switzerland).

ISO (**2012**). ISO 3745:2012, "Acoustics—Determination of sound power levels and sound energy levels of noise sources using sound pressure—Precision methods for anechoic rooms and hemi-anechoic rooms" (ISO, Geneva, Switzerland).

Koop, L., and Ehrenfried, K. (**2008**). "Microphone-array processing for wind-tunnel measurements with strong background noise," in *Proceedings of the 14th AIAA/CEAS Aeroacoustics Conference*, Vancouver, BC, Canada.

Ma, F., Abhayapala, T. D., and Samarasinghe, P. N. (**2023**). "A time-domain nearfield beamformer with spherical harmonic decomposition," J. Acoust. Soc. Am. **154**(3), 1850–1861.

Mao, Y., Gu, Y., Qi, D., and Tang, H. (**2012**). "An exact frequency-domain solution of the sound radiated from the rotating dipole point source," J. Acoust. Soc. Am. **132**(3), 1294–1302.

Mao, Y., Xu, C., Qi, D., and Tang, H. (**2014**). "Series expansion solution for sound radiation from rotating quadrupole point source," AIAA J. **52**(5), 1086–1095.

Merino-Martínez, R., Sijtsma, P., Snellen, M., Ahlefeldt, T., Antoni, J., Bahr, C. J., Blacodon, D., Ernst, D., Finez, A., Funke, S., Geyer, T. F., Haxter, S., Herold, G., Huang, X., Humprehys, W. M., Lecle?re, Q., Malgoezar, A., Michel, U., Padois, T., Pereira, A., Sarradj, E., Siller, H., Simons, D. G., and Sephr, C. (**2019**). "A review of acoustic imaging methods using phased microphone arrays: Part of the aircraft noise generation and assessment special issue," CEAS Aeronaut. J. **10**, 197–230.

Neise, W., and Michel, U. (**1994**). "Aerodynamic noise of turbomachines," Deutsche Forschungsanstalt Für Luft- Und Raumfahrt e.V., DLR, Institut Für Strömungsmechanik, Abt. Turbulenzforschung, Berlin, Germany.

Niu, X., Chen, H., Li, Y., Jia, X., Zhang, Y., Yong, X., and Li, C. (**2022**). "Design and performance of a small-scale acoustic wind tunnel at Wenzhou University for aerodynamic noise studies," Appl. Acoust. **199**, 109010.

Nolan, M., Berzborn, M., and Fernandez-Grande, E. (**2020**). "Isotropy in decaying reverberant sound fields," J. Acoust. Soc. Am. **148**(2), 1077–1088.

Ocker, C., and Pannert, W. (**2017**). "Imaging of broadband noise from rotating sources in uniform axial flow," AIAA J. **55**(4), 1185–1193.

Poletti, M., and Teal, P. (**2011**). "Comparison of methods for calculating the sound field due to a rotating monopole," J. Acoust. Soc. Am. **129**(6), 3513–3520.

Politis, A. (**2016**). "Microphone array processing for parametric spatial audio techniques," Ph.D. thesis, Aalto University, Espoo, Finland.

Pomberger, H., Sontacchi, A., Brandner, M., Resch, M., Brandl, S., and Höldrich, R. (**2016**). "Free-field pressure-based sound power measurement procedure with low spatial-sampling-and near-field-induced uncertainty," in *Proceedings of INTER-NOISE and NOISE-CON Congress and Conference Proceedings, Institute of Noise Control Engineering*, pp. 4318–4327.

Torija, A. J., Chaitanya, P., and Li, Z. (**2021**). "Psychoacoustic analysis of contra-rotating propeller noise for unmanned aerial vehicles," J. Acoust. Soc. Am. **149**(2), 835–846.

Torija, A. J., Li, Z., and Chaitanya, P. (**2022**). "Psychoacoustic modelling of rotor noise," J. Acoust. Soc. Am. **151**(3), 1804–1815.

Turhan, B., Jawahar, H. K., Gautam, A., Syed, S., Vakil, G., Rezgui, D., and Azarpeyvand, M. (**2024**). "Acoustic characteristics of phase-synchronized adjacent propellers," J. Acoust. Soc. Am. **155**(5), 3242–3253.

Vourakis, M., and Karlsson, M. (**2022**). "A round robin test of a low-pressure axial fan," in *Proceedings of FAN 2022*, Darmstadt, Germany, pp. 1–10.

Williams, E. G. (**1999**). *Fourier Acoustics: sound Radiation and Nearfield Acoustical Holography* (Academic Press, New York).

Zenger, F., Junger, C., Kaltenbacher, M., and Becker, S. (**2016**). "A benchmark case for aerodynamics and aeroacoustics of a low pressure axial fan," Tech. Rep. (SAE, Evanston, IL).

Zotter, F. (**2009**). "Analysis and synthesis of sound-radiation using spherical arrays," Ph.D. thesis, University of Music and Performing Arts, Graz, Austria.

Zotter, F., Sontacchi, A., Noisternig, M., and Höldrich, R. (**2007**). "Capturing the radiation characteristics of the bonang barung," in *Proceedings of the 3rd AAAA Congress*, pp. 27–28.